2014

Spectroscopy studies of straincompensated mid-infrared QCL active regions on misoriented substrates

Gregory Edward Triplett
Virginia Commonwealth University, getriplett@vcu.edu

Justin Grayer

Charles Meyer

Emily Cheng

Denzil Roberts

Spectroscopy studies of strain-compensated mid-infrared QCL active regions on misoriented substrates

Justin S. Grayer, Charles Meyer, Emily Cheng, Gregory Triplett, Denzil Roberts, et al.

Justin S. Grayer, Charles Meyer, Emily Cheng, Gregory Triplett, Denzil Roberts, Peter G. Schunemann, "Spectroscopy studies of strain-compensated mid-infrared QCL active regions on misoriented substrates," Proc. SPIE 8993, Quantum Sensing and Nanophotonic Devices XI, 89930T (31 January 2014); doi: 10.1117/12.2041073

SPIE.

Event: SPIE OPTO, 2014, San Francisco, California, United States

Spectroscopy studies of strain-compensated mid-infrared QCL active regions on misoriented substrates

Justin S. Grayer[1], Charles Meyer[1], Emily Cheng[1], Gregory Triplett[1], Denzil Roberts[1], and Peter G. Schunemann[2]

[1]Department of Electrical and Computer Engineering,
University of Missouri, Columbia, Missouri 65211

[2]BAE Systems, Nashua, NH 03061-0868

ABSTRACT

In this work, we perform spectroscopic studies of AlGaAs/InGaAs quantum cascade laser structures that demonstrate frequency mixing using strain-compensated active regions. Using a three-quantum well design based on diagonal transitions, we incorporate strain in the active region using single and double well configurations on various surface planes (100) and (111). We observe the influence of piezoelectric properties in molecular beam epitaxy grown structures, where the addition of indium in the GaAs matrix increases the band bending in between injector regions and demonstrates a strong dependence on process conditions that include sample preparation, deposition rates, mole fraction, and enhanced surface diffusion lengths. We produced mid-infrared structures under identical deposition conditions that differentiate the role of indium(strain) in intracavity frequency mixing and show evidence that this design can potentially be implemented using other material systems.

1. INTRODUCTION

There is a significant need for high power infrared lasers operating in the 3-5 μm spectral range. This range, along with 8-12 μm, is transparent in the atmosphere, thus opening up applications in communications, gas sensing, and defense. Conventionally, material bandgap determines wavelength; however, in multiple quantum well devices, such as quantum cascade lasers (QCL), quantum well thickness dictates emission wavelength. To achieve shorter emission wavelength, special consideration must be taken when designing the complete laser structure. For instance, zinc-blende alloys, which are typically employed in laser designs, are inherently nonlinear, due to their noncentrosymmetric nature. For this reason, substrate orientation is of particular importance to the performance of the laser device.

GaAs is a well-studied, mature nonlinear system. However, the (100) crystal orientation does not allow excitation of the nonlinear susceptibility for the transverse magnetic mode of emitted electromagnetic radiation[1]. Alternatively, the (111) crystal orientation offers many advantages such as higher packing density, greater strain tolerance, larger band discontinuity, and higher critical layer thickness[2]. Furthermore, frequency conversion is possible with InGaAs/AlGaAs grown on GaAs (111) due to the large ~7 % lattice mismatch of InAs with GaAs[3], which induces compressive strain and enhances the internal electric field in the system. Conversely, instead of the two dimensional structures needed for sharp transitions between quantum wells and cladding regions, InAs on GaAs (100) causes three dimensional or defect rich structures[3].

It should be noted that intracavity frequency mixing in quantum cascade lasers has been extensively studied and is well documented. Giovanni et al. reported successful synthesis of strained InGaAs/InAlAs on (111) InP substrates that took advantage of the lack of inversion symmetry inherent in zinc-blende structures to produce a frequency-doubled output beam[1]. Furthermore, in earlier work[3,4], we have observed second harmonic generation (SHG) in highly strained $In_{0.6}Ga_{0.94}As/Al_{0.45}Ga_{0.55}As$ QCLs grown on GaAs (111). Though marked success has been achieved with strain compensated structures, there are still significant challenges in producing mid-infrared frequency-doubled QCL devices.

Quantum Sensing and Nanophotonic Devices XI, edited by Manijeh Razeghi, Eric Tournié, Gail J. Brown,
Proc. of SPIE Vol. 8993, 89930T · © 2014 SPIE · CCC code: 0277-786X/14/$18 · doi: 10.1117/12.2041073

To keep the second harmonic amplitude on the order of and/or higher than the primary lasing mode, the refractive index at both wavelengths should be equal, i.e., the system must be phase-matched to produce the highest second harmonic conversion efficiency. Misoriented substrates, in which the crystal planes are periodically inverted, offer a convenient method for quasi-phase-matching in frequency mixed devices[5,6,7].

We report the observation of second harmonic generation by resonant Raman spectroscopy. Three active region AlGaAs/GaAs QCLs were simultaneously grown on GaAs (100) and (111) substrates by molecular beam epitaxy (MBE). Epitaxial growth on GaAs (111) requires careful sample preparation due to its narrow growth window[8]. Therefore, the purpose of these experiments was to determine the optimal growth conditions for GaAs (111) substrates. Growths were characterized by atomic force microscopy and photoluminescence spectroscopy to determine quality of the QCL structure. Using these results, strained InGaAs/AlGaAs QCLs with ten (10) and thirty (30) active regions were grown on orientation-patterned GaAs (OP-GaAs) (111) substrates, which were analyzed by resonant Raman spectroscopy.

2. SHG in nonlinear materials

When an electromagnetic field interacts with matter, a synchronous polarization field is produced by the excited electrons in the material[9]. This polarization wave interferes with the incident light assuming the two amplitudes are low and proportional. Linear optical phenomenon, such as refractive index, stem from these interference effects. Noncentrosymmetric materials exhibit asymmetric binding potentials. Elongated electron orbitals resulting from the lack of inversion symmetry are the mechanism behind higher order, nonlinear polarization effects. In this work, the focus remains on the second order, nonlinear polarization, which is directly proportional to $\chi^{(2)}$, the nonlinear susceptibility by the relation[9]:

$$P_{\chi}^{2\omega}(t) = \frac{\varepsilon_o}{2}\chi_{xzz}^{(2)}E_z^2 \exp(-2i\omega t) + c.c \tag{1}$$

Here, P is the polarization vector, ε_o is the permittivity in vacuum, $\chi^{(2)}$ is the second orde, nonlinear susceptibility, E is the time varying electric field component of the incident electric field assuming the incident field is perpendicular to the medium, and ω is the frequency of the incident electromagnetic field; c.c. is simple notation for the complex conjugate of the previous terms[9]. Maximization of the dipole matrix element while simultaneously minimizing energy dispersive effects is paramount to optimizing nonlinear susceptibility[1,3,4,6-7,9-11] given by the following:

$$\chi^2(2\omega) = \frac{e^3}{\varepsilon_o}N\frac{<z_{i-ii}><z_{ii-iii}><z_{iii-i}>}{(\hbar\omega-\Delta E_{i-ii}-i\Gamma_{i-ii})(2\hbar\omega-\Delta E_{i-iii}-i\Gamma_{i-iii})}; \tag{2}$$

where electron density in the active region is given by N, ΔE is the energy separation between subband states, Γ_{ij} and $<z_{ij}>$ are the half width at half maximum and the matrix element of the i-j intersubband transition, respectively. The difference in nonlinear properties between zinc-blende (100) and (111) oriented crystals can be understood by examining the electric field matrix elements of the polarization vector[1]:

$$\begin{pmatrix} P_x \\ P_y \\ P_z \end{pmatrix} = \varepsilon_o \begin{pmatrix} 0 & 0 & 0 & d_{14} & 0 & 0 \\ 0 & 0 & 0 & 0 & d_{14} & 0 \\ 0 & 0 & 0 & 0 & 0 & d_{14} \end{pmatrix} \begin{pmatrix} E_x^2 \\ E_y^2 \\ E_z^2 \\ 2E_yE_z \\ 2E_zE_x \\ 2E_xE_y \end{pmatrix}; \tag{3}$$

with d_{14} being the nonlinear coefficient of the nonlinear susceptibility. For (100) substrates $\mathbf{E}=\mathbf{E_z}$ which leads to a null polarization vector. Conversely, the electric field vector in (111) crystal planes is $\mathbf{E}=\mathbf{E_x}+\mathbf{E_y}+\mathbf{E_z}$, resulting in a nonzero

polarization. For orientation-patterned substrates, the coherence length of the second harmonic is extended due to the periodic inversion of the crystal planes. Conversion efficiencies of greater than 30% have been reported[6] with a nonlinear coefficient of ~94pm/V[6,7]. Utilization of orientation-patterned oriented substrates is still in their infancy, due to the extremely rare manner in which they are produced[7,12]. Thick OP-GaAs layers have been grown by hydride vapor epitaxy, however due to the rarity of this technique, orientation-patterned substrates are more expensive[12], which inhibits their widespread use.

3. Theoretical treatment

The unipolar nature of QCLs allows them to be modeled using the single band envelope approximation[4,13-15] of the Krönig-Penny model, which predicts intersubband electronic transitions with high accuracy. In this approximation, the wave functions in the quantum wells are the product of periodic Bloch wave functions and slowly time varying envelope functions. Assuming opposite parity, optical transitions are allowed between envelope states[13]. To be sure, the dipole corresponding to the transition between the conduction and valence band occurs between Bloch states[14]. In this configuration, the envelope function is kept constant; however, in interband transitions, the Bloch functions are kept constant allowing the dipole to occur between envelope states.

QCLs are unique in that more than one photon can be produced per excited electron. Quantized electronic states arise if the width of the barrier regions near the quantum wells is less than that of the de Broglie wave function[9]. In this case, electron confinement occurs in the direction normal to the growth planes. Moreover, the electrons are free to move in the in-plane direction, which is important for the cascading effect. Applying a normal electric field ($\mathbf{E}_z$) to the QCL structure causes a Stark effect in which electronic states are broadened. Furthermore, band bending occurs causing electron motion from one active region to the next[4]. Radiative processes in QCLs are conventionally associated with the E_3-E_2 transition[3]. Immediately following, the electron undergoes a thermal transition (E_2-E_1) resulting in the generation of a phonon. Due to the lowered energy of the barrier region caused by band bending, the electron tunnels to the adjacent active region where the process repeats itself. Photon emission, and therefore optical power, is proportional to the number of active regions and carrier density.

From the familiar wavelength-energy relation, it can be easily seen that intersubband transitions result in longer wavelength. To extend the laser transition to shorter mid-infrared wavelengths, second harmonic generation has been modeled on GaAs (111) orientation using a self-consistent Schödinger-Poission solver. The QCL structure simulated can be seen in Figure 1[3-4].

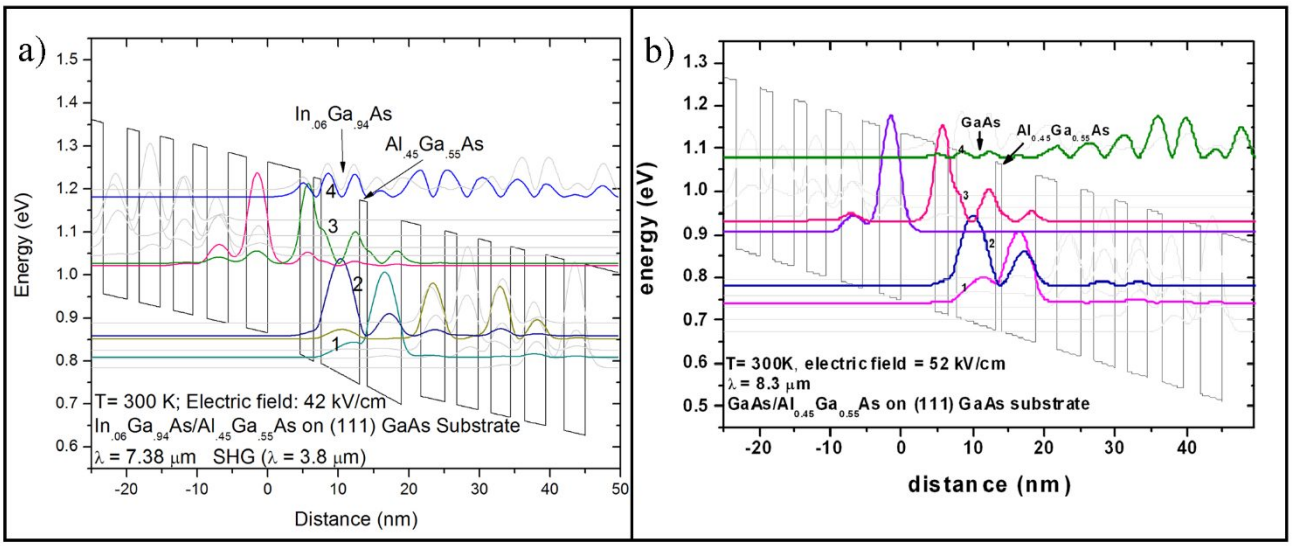

Figure 1. Simulation QCL device using a self-consistent Schrödinger-Poisson solver; a) asymmetric well geometry casused by compressive strain of the 7% lattice mismatched $In_{0.06}Ga_{0.94}As$ quantum well results in a lower fundamental emission wavelength, as well as SHG. Conversely, the unperturbed wells in the GaAs/AlGaAs has longer emission wavelength, and does not exhibit SHG

A three InGaAs quantum well configuration was employed for this study. The injector region consisted of several alternating GaAs/AlGaAs layers. Layer widths in nm from substrate on are as follows: 2.8, **3.4** 1.7, **3.0**, 1.8, **2.8**, 2.0, **3.0**, 2.6, **3.0**, 4.6, **1.9**, 1.1, **5.4**, 1.1, **4.8**. Here, GaAs layers in the injector region are bold only, while the three InGaAs quantum wells are bold and underlined. With 6% indium in the quantum wells, a notable alteration in the InGaAs quantum wells results in a blue shifted fundamental wavelength (7.38μm) as compared to that of an AlGaAs/GaAs quantum well configuration (8.3μm) with identical dimensions. This comes by way of the induced E_4 intersubband, and the E_4-E_2 transition. Our simulation shows the SHG wave of the InGaAs system, which occurs at 3.8 microns. Also of note is the significantly reduced amplitude of the electric field in the InGaAs/AlGaAs QCL compared to that of the AlGaAs/GaAs structure. This reduction in the applied electric field required for band bending is due to the strain-induced enhancement of the inherent electric field in both InGaAs and GaAs (111) caused by the piezoelectric effect.

4. Experiment

Si doped GaAs (111)B substrates 2° offset toward the <2-1-1> direction were prepared using the method proposed by Elcess et al[8]. Degreasing of the substrates was carried out using an AMD (acetone, methanol, DI water) wash. Immediately following, the substrate was submerged in a 65°C sulfuric acid bath for ten (10) minutes, followed by a room temperature sulfuric acid bath for another ten (10) minutes. Finally, the substrate was etched in 5:1:1 H_2SO_4: H_2O_2:H_2O for forty (40) minutes to remove the oxide layer and OH-terminate the surface. This OH termination makes the substrate layer highly hydrophobic, which should lead to longer diffusion lengths during growth. Furthermore, this method of sample preparation leads to a significantly decreased oxide desorption during MBE growth. GaAs (100) has a large growth window and shows little change in growth parameters when etched[8]. Therefore, GaAs (100) wafers were not etched, but were used to observe reflection high-energy electron diffraction during growth. Both (100) and (111) wafers were indium-mounted on the same molybdenum sample blocks, and AlGaAs/GaAs QCLs with three active regions were simultaneously grown in a Varian Gen II solid-source MBE. Gallium growth rate estimated from beam equivalent pressure (BEP) was 0.81Å/s, while aluminum growth rate was 0.72Å/s, leading to an $Al_{0.45}Ga_{0.55}As$/GaAs structure. The V:III (As:Ga/Al) (BEP) was kept constant at ~24:1.

It should be noted that the GaAs (111)B 2° offset toward <2-1-1> wafers after etching proved difficult to determine desorption temperature, due to the removal of the oxide layer. Furthermore, degradation of the (111) surface occurs immediately after oxide desorption (~580°C) if growth does not commence immediately[8]. Similar to Ecless et al[8], a two-step growth process was followed in which several monolayers were deposited at a lower temperature followed by raising the substrate temperature to the final growth temperature. Thus, using proven, successful growth parameters from earlier studies, we varied both the "protective layer" deposition temperature and the final growth temperature from 540-570°C and 590-610°C, respectively. Growths were analyzed by AFM, photoluminescence spectroscopy, and Raman spectroscopy to determine sample quality. The goal of this experiment was to determine the optimum growth parameters for growing QCLs on GaAs (111) substrates to be used to grow on OP-GaAs samples; therefore, AFM was not performed on GaAs (100) substrates.

AFM analysis was performed on a $10\mu m^2$ area of the GaAs (111) QCL samples. Optimal growth temperature was found to be between 540-550 °C for the 10 monolayer (ML) protective layer, and as high as 610°C for the final growth temperature. An RMS roughness of 0.053 nm was obtained for the smoothest sample, grown with the temperatures of 550°C and 610°C for the protective and final growth temperatures, respectfully. Table 1 contains the growth parameters for the three samples that produced the lowest AFM RMS surface roughness.

Table 1. Growth Parameters for Samples that produced Lowest AFM RMS Surface Roughness

10 ML initial growth temperature (^{o}C)	Final growth temperature (^{o}C)	RMS surface roughness of a 10μm^2 area (nm)
550	610	0.0533
540	600	0.0567
540	590	0.08

Further analysis of MBE-grown QCL structures was achieved using PL and Raman spectroscopy. Figure 2 contains the PL spectrum obtained from both the GaAs (111)B 2^{o} offset and (100) QCL structures. Both the (111)B 2^{o} offset and (100) structures show two distinct features. The first peaks located at 859.4nm (111) and 874.6nm (100) are at the fundamental conduction-to-heavy hole transition of GaAs. We associate the second major peak at 786.8nm (111) and 787.4nm (100) with the characteristic blue shift of sequential quantum wells[15]. Moreover, this image of the two-dimensional density of states indicates excellent epitaxial layers. Also noteworthy is the dramatic increase in signal intensity from GaAs (100) to (111)B substrates. The peak associated with the joint density of states is much more pronounced compared to the fundamental GaAs mode in the AlGaAs/GaAs QCL on (100), while in the (111)B system, the peak-to-peak are very comparable to each other. These discrepancies between the (100) and (111)B AlGaAs/GaAs QCLs could possibly be from the inherent piezoelectric property of GaAs (111), however we did not see such enhanced electric fields in our simulation.

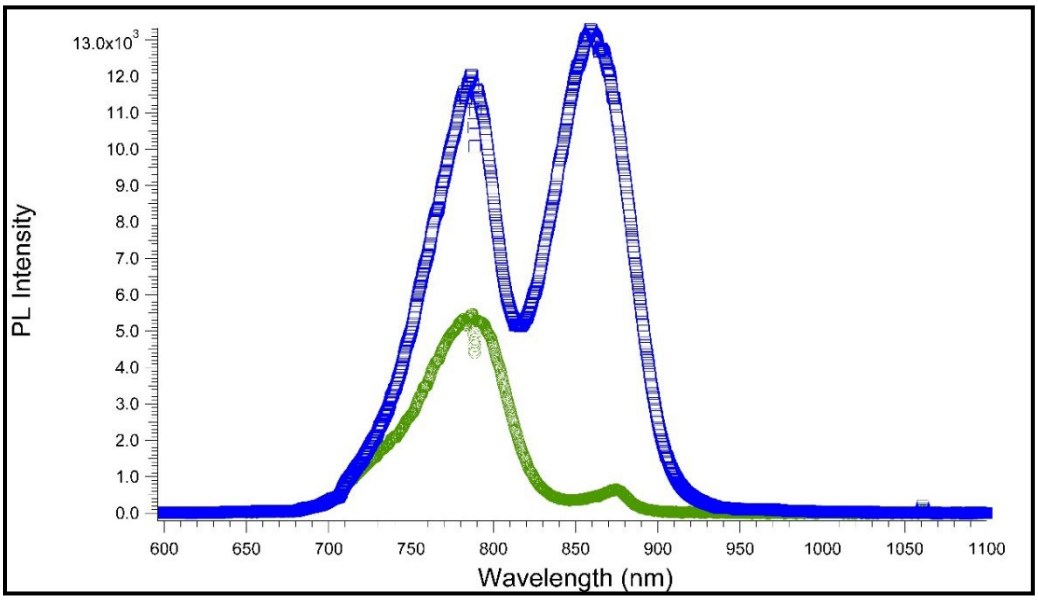

Figure 2. PL spectra obtained from AlGaAs/GaAs QCL from 600-1100 nm. QCL grown on GaAs (111)B (top, □) substrate shows much greater signal than that of the GaAs(100) (bottom, ○) substrate. In both spectra, the joint density of states is seen ~787 nm, indicating successful two-dimensional growth of a series of quantum wells.

Raman spectra was also taken on these three active region QCLs. Figure 3 shows the Raman spectra obtained from both GaAs (100) and (111)B 2^{o} offset AlGaAs/GaAs QCLs. Most notable is the shift in intensity of the LO (289.43cm^{-1}) and

TO (267.24 cm^{-1}) phonons of GaAs from the (111) spectra to the (100) spectra. Moreover, the same shift occurs in the LO (391cm^{-1}) and TO (359cm^{-1}) phonons of AlAs. These values for the LO and TO phonons of both GaAs and AlAs are in good agreement with earlier studies[3] and examples found in the literature[16].

Using the optimized parameters from the (111)/(100) AlGaAs/GaAs study, we grew InGaAs/AlGaAs QCL structures on OP-GaAs substrates with an orientation inversion period of 69μm. Indium growth rate was 0.08Å/s to yield an indium content of ~10%. Ten and thirty active region QCLs were grown by MBE, and analyzed using resonant Raman spectroscopy to observe intersubband transitions.

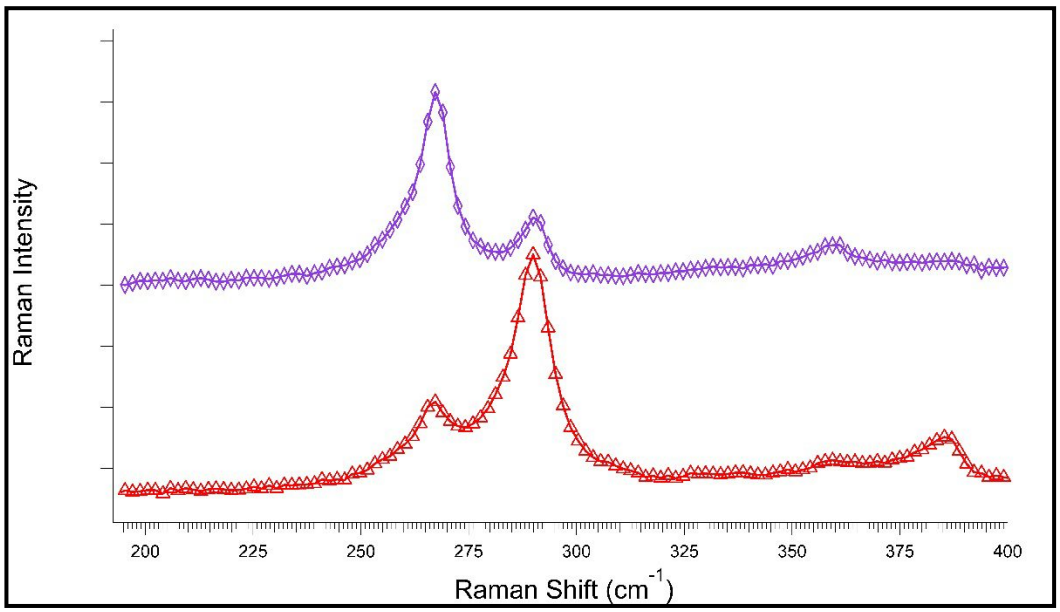

Figure 4. Raman spectra obtained for 3 active region AlGaAs/GaAs QCLs simultaneously grown on GaAs (100) (top,Δ) and (111)B 2° (bottom, ◊) offset by MBE. LO (289.93cm^{-1}) and TO (267.24cm^{-1}) phonons of GaAs clearly switch intensity with crystal orientation in close agreement with earlier studies[3]. LO (391cm^{-1}) and TO (359cm^{-1}) phonons of AlAs follow a similar trend. Spectra offset to enable simultaneous comparison.

5. Results and discussion

Figure 5 shows results from resonant Raman spectroscopy on $In_{0.1}Ga_{0.9}As/Al_{0.45}Ga_{0.55}As$ QCL lasers grown on an orientation-patterned GaAs (111) wafer with a crystal inversion period of 69μm. Raman was taken on a Renishaw RM-series micro Raman spectrometer at 5X magnification. The excitation beam was the 514.5 nm line of an Ar-ion laser. Integration time was thirty seconds, and five successive scans were averaged together to give a higher signal to noise ratio. 5X magnification was used to illuminate and excite the maximum number of inversion periods. Furthermore, at 20X and 50X magnification, higher energy features were not observed. With 20X and 50X magnification, LO and TO phonon energy levels dominate, drowning out higher spectral resonances. Spectrum was normalized and peak fit using a binomial smoothing algorithm.

In addition to the LO and TO phonon modes previously mentioned, at 124.38 cm^{-1} we also observe a sharp Raman peak; however, we attribute this to cosmic ray aberrations. Therefore, we treat this peak as negligible. Matsumoto et al reported the first intersubband transition of GaAs at 540 cm^{-1} as observed by Raman spectroscopy and attenuated total reflection spectroscopy[17]. We detect a similar intersubband peak at 502 cm^{-1}. We attribute this peak to a red shifted E_{21} transition from the InGaAs quantum wells caused by higher temperature (300K) measurements than those reported by

Mastumoto[13]. Further, Matsumoto proposed that intersubband excitations can couple with LO phonons to produce coupled-collective modes. In addition to the lower frequency mode associated with the E_{21} transition of the InGaAs quantum wells, the higher mode located in our data at 793.31cm^{-1} is associated with an effective plasma energy, E_p[17]. Using these two energies (E_{21}=62.35eV and E_p=98.42eV) we can estimate the oscillator strength by the relation

$$S_{12} = \frac{E_p^2}{E_{12}^2}\varepsilon_{GaAs,\infty}. \quad (4)$$

For our QCLs, we estimate an oscillator strength of ~27 using the value of $\varepsilon_{GaAs,\infty}$=10.79. At 4.2K, Harbeke reported intersubband transitions from GaAs/AlGaAs Quantum wells at ~120meV[13]. The dominant peak in our Raman data at 118 meV is very similar to this value. The prominence of this peak in the spectrum is most likely due to the large number of AlGaAs/GaAs regions in the many injector layers of these QCLs. In close agreement with the modeled QCL structure, we see a laser peak associated with the E_{32} transitions at 1376cm^{-1}, which yields a fundamental wavelength of 7.293µm. We attribute a second harmonic of this fundamental mode at 2329cm^{-1}, which corresponds to a laser line of 4.3µm (E_{42} transition)[3]. Furthermore, this mode has a normalized intensity greater than that of the fundamental mode; therefore, the OP-GaAs substrates have the potential for quasi-phase matching to increase the second harmonic laser line. There seems to be another mode close to the fundamental mode at 1565.2cm^{-1},which we attribute to another laser mode at 6.39µm To be sure, a second harmonic of this mode is present at 3.96µm (2521cm^{-1}).

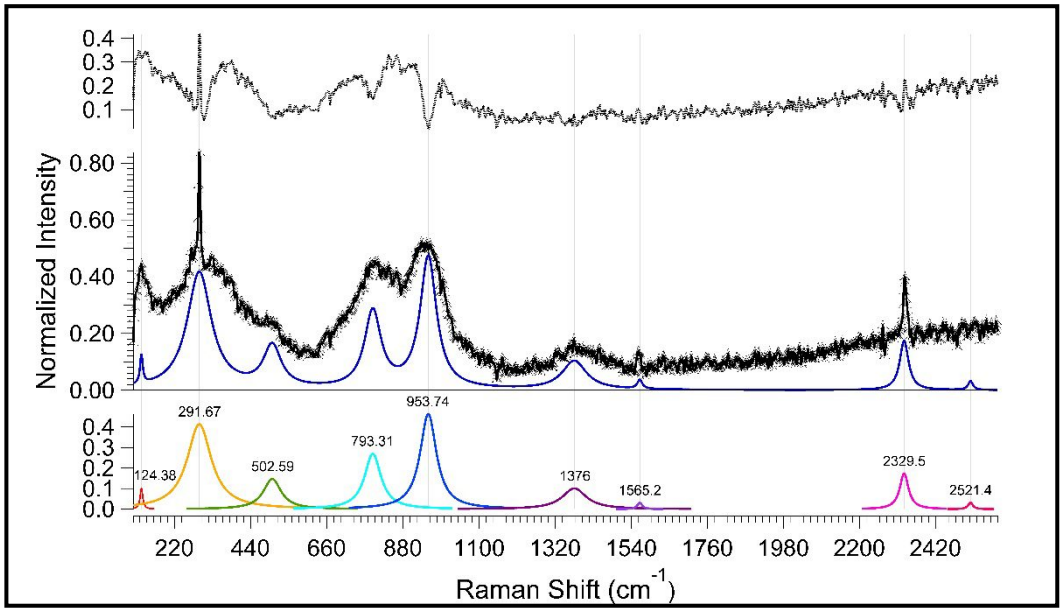

Figure 5. Peak fit resonant Raman spectra of a 10 active region OP-GaAs based $In_{0.1}Ga_{0.9}As/Al_{0.45}Ga_{0.55}As$ QCL. Oscillator strength of S_{12}=27 obtained from E_{21} and E_p at 502.59cm^{-1} and 793.31cm^{-1}, respectively. Intersubband transitions observed from AlGaAs/GaAs injector regions observed at 953.74cm^{-1}. Two fundamental modes of 7.3µm and 6.4µm observed, as well as their second harmonics at 4.3µm and 3.96µm, respectively. Upper spectrum is the difference between the raw and fitted data, Lower spectrum are the fitted peaks with their respective positions.

6. Conclusion

We determined the optimal growth temperature for successful epitaxial growth by MBE on GaAs (111)B 2^o offset toward the <2-1-1> substrates. Comparison between the properties of QCLs on semi-insulated GaAs (100) and GaAS(111)B 2^o offset toward the <2-1-1> plane were discussed as demonstrated using PL and Raman spectroscopy. Using the results from our preliminary (100)/(111) study, we successfully grew InGaAs/GaAs QCL structures on OP-GaAs substrates. These substrates offer both enhanced electric fields do to the piezoelectric effect inherent in strained GaAs (111) substrates, as well as the potential for quasi-phase matching do to the periodic inversion of the crystal

orientation. Through resonant Raman spectroscopy, we observed both SHG and quasi-phase matching in ten active region InGaAs quantum wells in agreement with theoretical models.

Acknowledgements

This work was supported by AFOSR Young Investigator Program Grant Number FA9550-10-1-0482.

References

[1] Giovannini, M., Beck, M., Hoyler, N., and Faist, J., "Second harmonic generation in (111)-oriented InP-based quantum cascade laser", Journal of Applied Physics, **101**, 102107 (2007)
[2] Anan, T., Nishi, K., and Sugou, S., "Critical Layer thickness on (111)Boriented InGaAS/GaAs heteroepitaxy", Applied Physics Letters, **60**, 3159 (1992)
[3] Meyer, C., Cheng, E., Grayer, J. Meueller, D. Triplett, G., Roberts, D., "Pseudomorphic growth of InAs on misoriented GaAs for extended quantum cascade wavelength", J. Vac. Sci. Technol. A., Vol. 31, No. 6, (Nov/Dec 2013)
[4] Roberts, D [Gallium Arsenide-Based Quantum Cascade Lasers for Mid-Infrared Operation at 3-5 Micron Grown by Molecular Beam Epitaxy], Doctoral Dissertation, University of Missouri, Columbia, MO. Ch. 4-6, (2011)
[5] Sanchez, J.J., Tijero, J.M.G., Hernando, J., Sanchez-Rojas, J.L., Izpura, I., "Optical Investigation of the relaxation process in InGaAs/GaAs ingle quantum wells grown on (001) and (111)B GaAs substrates", Microelectronics Journal, 30, 363-366 (1999)
[6] Skauli, T., Vodopyanov, K. L., Pinguet, T. J., Schober, A., Levi, O., Eyres, L. A., Fejer, M. M., Harris, J. S., et al "Measurement of the nonlinear coefficient of oriented-patterned GaAs and demonstration of highly efficient second harmonic generation", Optics Letters, vol. 27, No. 8, (2002)
[7] Schunemann, P. G., Pomeranze, L. A., Young, Y. E., Mohnkern, L., and Vera, A. "Recent advances in all-epitaxial growth and properties of orientation-patterned gallium arsenide (OP-GaAs)", CWJ5, OSA/CLEO/IQEC (2009)
[8] Elcess, K., Lievin, J. L., and Fonstad, C. G., "Growth of GaAs, AlGaAs, and InGaAs on (111)B GaAs by molecular-beam epitaxy", J. Vac. Sci. Technol. B, 6 (2), 638-641 (Mar/Apr 1988)
[9] Rosencher, E., Fiore, A., Vinter, B., Berger, V., Bois, Ph., and Nagle, J., "Quantum Engineering of Optical Nonlinearities", Science, New Series, vol. 271, no. 5246, 168-173 (1996)
[10] Capasso, F., Sirtori, C., Cho, A. Y., "Coupled Quantum Well Semiconductors with Giant Electric Field Tuanable Nonlinear Optical Properties in the Infrared". IEEE Journal of Quantum Electronics, vol. 30, no. 5, 1313-1326 (1994)
[11] Bester, G., Wu, X., Vanderbilt, D., Zunger, A., "Importance of Seond-Order Piezoelectric Effects in Zinc-Blende Semiconductors", PRL **96**, 1976-2 (2006)
[12] Bliss, D. F, Lynch, C., Weyburne, D., O'Hearn, K., Bailey, J. S., "Epitaxy growth of thick GaAs on orientation-patterned wafers for nonlinear optical applications", Journal of Crystal Growth, 287, 673-678 (2006)
[13] Harbeke, G., "Intersubband Spectroscopy of Semiconductor Quantum Wells", Physica Scripta, vol.T29, 135-140 (1989)
[14] West. L. C., Eglash, S. J., "First observation of an extremely large dipole infrared transition within the conduction band of a GaAs quantum well", Applied Physics Letters, **46**, 1156 (1985)
[15] Faist, J., [Quantum Cascade Lasers], Oxford University Press, Great Clarendon Street, Oxford, OX 2, 6DP, United Kingdom. Ch1 (2013)
[16] Berdekas, D. and Ves, S., "Lattice Dynamics and Raman scattering by phonons of GaAs/AlAs (001) superlattices", J. Phys.:Condens. Matter, **21**, 275405 (2009)
[17] Matsumoto, T., Haraguchi, M., Fukui, M., Yamaguchi, M., Kubo, H., Hamaguchi, C., and Nakashima, S., "Experimental Observation of Intersubband Excitations in Si-Doped GaAs/AlAs Multiple Quantum Wells", Jpn. J. Appl. Phys., vol 34, 2241-2246 (1995)